GEOPHYSICS, VOL. 65, NO. 1 (JANUARY-FEBRUARY 2000); P. 247–252, 6 FIGS.

Imaging shallow objects and heterogeneities with scattered guided waves

Gérard C. Herman*, Paul A. Milligan‡, Robert J. Huggins**, and J. W. Rector§

ABSTRACT

Current surface seismic reflection techniques based on the common-midpoint (CMP) reflection stacking method cannot be readily used to image small objects in the first few meters of a weathered layer. We discuss a seismic imaging method to detect such objects; it uses the first-arrival (guided) wave, scattered by shallow heterogeneities and converted into scattered Rayleigh waves. These guided waves and Rayleigh waves are dominant in the shallow weathered layer and therefore might be suitable for shallow object imaging. We applied this method to a field data set and found that we could certainly image meter-size objects up to about 3 m off to the side of a survey line consisting of vertical geophones. There are indications that cross-line horizontal geophone data could be used to identify shallow objects up to 10 m offline in the same region.

INTRODUCTION

Both electromagnetic (EM) and seismic methods are used for imaging the shallow subsurface. An overview of the use of current seismic reflection imaging methods in the shallow subsurface is given by Steeples et al. (1997). These shallow seismic reflection methods are in effect similar to those used in the petroleum exploration and production industry but are scaled down in size; shotpoint offsets are much reduced, smaller charges or weight-drop sources are used, and geophone spacings as short as 0.5 m (or less) are used to prevent spatial aliasing of Rayleigh waves and airwaves. Use of the surface seismic reflection method, based on common-midpoint (CMP) reflection gathers and stacking to image the very shallow subsurface, is often limited by the early record times being dominated by different types of strong and coherent guided-wave modes trapped in the weathered layer. Examples of these guided waves are Rayleigh waves and the first arrivals refracted at a shallow interface and reflected multiple times by the free surface.

In this paper, we present a method for imaging acoustic impedance heterogeneities in the shallow weathered layer by using these strong guided-wave modes. In a field experiment, we buried an empty drum to act as a secondary source of scattered Rayleigh waves and used the first arrival as the illuminating wave. We then processed the data to see if we could detect the drum.

An earlier paper (Blonk et al., 1995) demonstrated that Rayleigh waves can be used to image a large object (a dam) at a distance of 150 m in a tidal flat region. It appeared possible to image scatterers in a karstified near-surface region at distances of more than 1 km. In our paper, we concentrate on imaging small (meter-size) objects at relatively close distances from the receivers (typically <10 m) in a region where a significant amount of very shallow near-surface scattering takes place. The fact that we are now dealing with near-field scattering effects, where the distance between scattering objects and receivers is typically a few wavelengths (or less), has consequences for the data processing method, which are outlined in this paper.

DESCRIPTION OF THE METHOD

We consider scattering of guided waves by shallow subsurface inhomogeneities that are relatively small with respect to the wavelength. The wavefield is generated by a source at surface position $\mathbf{x}^s$ and is recorded by vertical geophones at surface position $\mathbf{x}$. Starting from the frequency-domain form of the elastodynamic wave equation, one can derive a domain-type integral representation for the vertical component of the

Published on Geophysics Online November 17, 1999. Manuscript received by the Editor February 13, 1998; revised manuscript received December 21, 1998.
*Center for Tech. Geoscience, Delft Univ. of Technology, Mekelweg 4, 2628 CD Delft, Netherlands; E-mail: g.c.herman@math.tudelft.nl.
‡Lawrence Berkeley National Laboratory, Univ. of California–Berkeley, Bldg. 90, Rm. 2002, Berkeley, California 94270; E-mail: paul@hmbrt.lbl.gov.
**GeoMetrics Inc., 2190 Fortune Dr., San Jose, California 95131; E-mail: rob@mail.geometrics.com.
§Dept. of Materials, Science and Mineral Engineering, Univ. of California–Berkeley, 577 Evans Hall, Berkeley, California 94270; E-mail: jwrector@lbl.gov.

particle velocity, v:

$$v(\omega, \mathbf{x}, \mathbf{x}^s) = v^0(\omega, \mathbf{x}, \mathbf{x}^s) + v^1(\omega, \mathbf{x}, \mathbf{x}^s) , \qquad (1)$$

where ω denotes the angular frequency, the incident field v^0 is the wavefield that would be present in the absence of scattering objects, and the scattered field v^1 accounts for the presence of these objects. In our case, the offset between shot location and nearest receiver is chosen large enough so that the first arrival is separated in time from the airwave and Rayleigh-wave modes. This first arrival can be a refracted wave that, after multiple bounces at the free surface, has become a guided wave, propagating mainly in the layer above the refracting interface. We consider the first arrival as the incident field. For shallow objects, the scattered field can be expressed in terms of the scattering impedance ξ by the relation

$$v^1(\omega, \mathbf{x}, \mathbf{x}^s) = \int_{\text{surface}} dA(\mathbf{x}')\xi(\omega, \mathbf{x}')V^G(\omega, \mathbf{x} - \mathbf{x}')v(\omega, \mathbf{x}', \mathbf{x}^s), \qquad (2)$$

where the Green's function V^G is the vertical velocity resulting from an impulsive vertical point force. In equation (2), we have essentially lumped all scattering processes at the surface. This seems reasonable, since we expect that the Rayleigh waves, which are the dominant part of V^G, are mainly concentrated in the upper few meters of the subsurface. In equation (2), we also assume that the near surface, apart from the scattering objects (the background), is laterally invariant. The validity of this type of scattering model is discussed by Blonk et al. (1995). In principle, shallow scattering objects can now be determined by carrying out three steps.

First, separate the incident wave v^0, in our case the first arrival, and the scattered wave v^1. For scattering objects close to the receivers, these can interfere and must be separated by the same type of wavefield separation techniques used in processing vertical seismic profiling (VSP) and crosswell reflection data.

Second, determine the Green's function V^G. Since near-surface scattered waves predominantly consist of Rayleigh waves (Blonk and Herman, 1994), the Rayleigh-wave part is especially important here. In principle, this part can be measured in the field directly by recording the short offsets. In our experiment, however, these short offsets were not available and a modeling approach was used.

After determining the scattered field and the Green's function, the impedance function ξ can be determined in a way similar to seismic migration (see, for instance, Berkhout, 1985), the main difference being that the incident field is the first arrival and the scattered field is a Rayleigh wave. After removing the wave propagation effect from the source to an imaging point $\mathbf{x}$ and from this imaging point to the receivers, the image of the scattering impedance at location $\mathbf{x}$ is found at time $t = 0$.

The determination of the Green's function at all surface locations to be imaged can be computationally intensive. Later, we discuss a number of simplifications concerning computing the Green's function and imaging the scattered field. These simplifications are intimately related to the acquisition geometry used.

DESCRIPTION OF THE EXPERIMENT

The experiment was carried out at the Richmond Field Station of the University of California at Berkeley. The terrain, situated in the San Francisco Bay margin, can be characterized as a muddy wetland, overgrown with grass and a few small bushes. The upper 30 m of the subsurface consist of tertiary muds; the water table is at approximately 3 m depth. The objective was to investigate to what extent meter-size objects could be detected in the shallow subsurface using the technique of guided-wave imaging.

The data-acquisition geometry is shown in Figure 1. The receivers were laid out in a straight line with a spacing of 0.5 m. Both vertical and cross-line horizontal geophones were used. A vertical impact, in-line Betsy gun (8-gauge shells) was used as a source. The experiment using the vertical phones was carried out twice. First, shot records were recorded for six different shot positions spaced 10 m apart; the closest shot was situated 40 m from the first receiver. Then, an empty plastic drum about 0.6 m in diameter and about 1 m long was buried 10 m away and 1 m deep (oriented parallel to the line), after which the experiment was repeated with the same shot locations as before. The objective of this experiment was to compare the strength of the scattered field as a result of the drum with other near-surface scattering effects. For example, a bush about 1 m in diameter was present about 3 m from the line. The position of the bush is also shown in Figure 1. We also intended to perform the same pair of before-and-after experiments for the cross-line horizontal components but, because of equipment failure and lack of time, we were only able to record the cross-line horizontal data after the drum burial.

PROCESSING AND INTERPRETATION OF THE VERTICAL COMPONENT DATA

The processing sequences of the two vertical component data sets (before versus after drum burial) were identical and consisted of following steps.

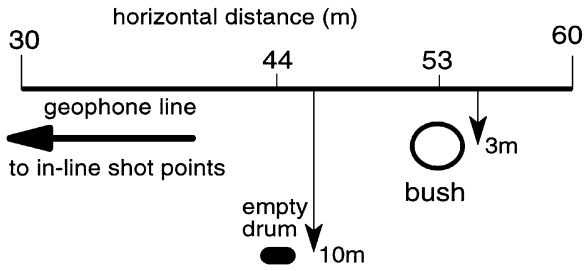

FIG. 1. Plan view of the Richmond Field Station experiment. The objective was to investigate to what extent meter-size objects could be detected in the shallow subsurface using the technique of guided-wave imaging. The receivers were laid out in a straight line with a spacing of 0.5 m (all horizontal distances are measured with respect to the first receiver). Both vertical and cross-line horizontal geophones were used. The experiment using the vertical phones was carried out twice: both before and after burying an empty plastic drum of about 0.6 m diameter and 1 m tall. The cross-line horizontal data were recorded only after burying the drum. Shot records were recorded for six different shot positions spaced 10 m apart; the closest shot was situated 40 m from the first receiver.

Separation of the incident and scattered waves

A shot record, representative of the vertical component data both before and after burying the drum, is shown in Figure 2. There was no apparent difference between the before-and-after shot records to indicate the presence of scattered waves from the drum; thus, the dominant first arrival was removed to enhance the presence of the scattered wavefield. Before removing the first arrival, receiver statics were determined by picking first-break arrival times and subsequently were removed by aligning traces on the first-break times. Then, the first-arrival wave was subtracted out using a constrained eigenvector wavefield separation technique (Mars and Rector, 1995), leaving behind the scattered Rayleigh waves. More details on this important preprocessing step can be found in the discussion of Figure 4.

Determination of the Green's function

In principle, the Rayleigh-wave part of the Green's function V^G can be measured in the field directly by recording the short offsets. In our experiment, however, these short offsets were not available and a modeling approach was used. Since we only imaged at the receiver locations (discussed in more detail below), we only needed the Green's function from scattering points at the receiver line to the receivers themselves. We did not attempt an accurate true-amplitude imaging, and we settled for a Green's function of the form

$$V^G(\omega, x - x') = \mathrm{e}^{-\mathrm{j}\omega|x-x'|/c_R}, \tag{3}$$

where c_R is the Rayleigh-wave velocity observed in the data, x is the receiver coordinate along the line, and x' is the imaging point along the line. This Green's function is kinematically correct for a particular Rayleigh-wave mode but does not account for the proper amplitude behaviour. To remedy this somewhat, we have taken the Rayleigh-wave velocity to be complex valued, i.e.,

$$c_R = |c_R|(1 + \mathrm{j}\alpha) \quad (\alpha \geq 0), \tag{4}$$

with $\alpha = 0.1$. In this way, the amplitude decay of the Green's function was similar to the decay visible in the field data within the frequency range of interest.

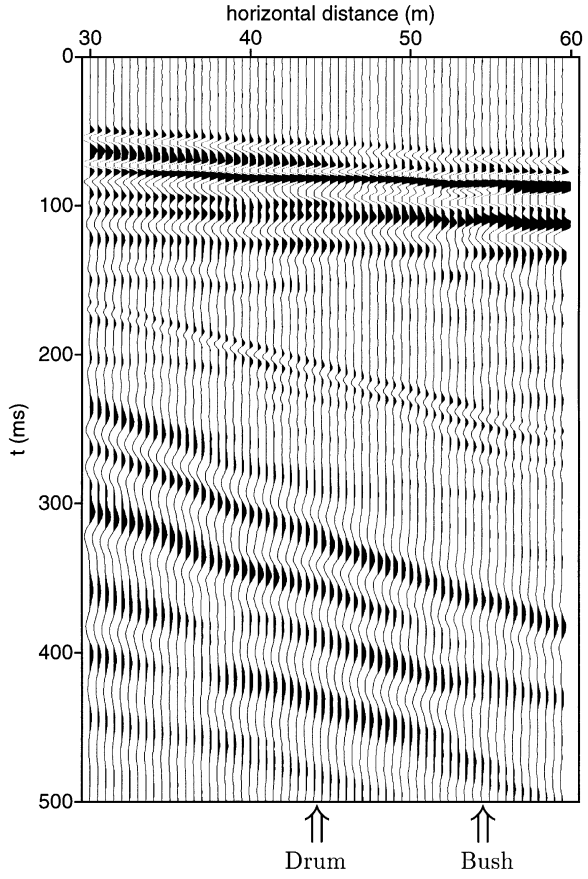

FIG. 2. A shot record, representative of the vertical-component data sets. The horizontal distance is measured with respect to the first receiver. The first arrival occurs at about 80 ms, the airwave starts at about 180 ms, and the low-frequency ground roll (Rayleigh wave) starts at about 270 ms.

Imaging of the impedance function

To obtain an image of the scattering impedance function ξ, wave propagation effects from the sources and receivers to all surface locations must be compensated for, followed by an imaging step at time $t = 0$. In the frequency domain, this can be achieved by summing the result after wavefield extrapolation over all frequencies (Berkhout, 1985). This type of approach is also taken in Ernst and Herman (1998) for the case of scattered guided waves. For the imaging problem considered here, we are only interested in imaging objects closer than, say, 10 m from the line (which amounts to only one or two wavelengths of the dominant frequency of the scattered Rayleigh waves) and a less computationally intensive approach is possible if the velocities do not change too much over this short distance.

As a first step, propagation effects of the guided wave from the source to all points to be imaged must be removed. For the shots of interest, the path length from the in-line sources to a point at position (x_1, y_1) (with $y_1 < 10$ m) differs $<5\%$ of the dominant wavelength from the path length from the source to the receiver at $(x_1, 0)$. Hence, we can remove propagation effects from the source by correcting for the first-arrival times already determined in the first step of wavefield separation. Figure 3 shows the total wavefield, v, after removing propagation effects from the source to the points to be imaged and adding the results for the different sources (for the data set recorded after the burial of the drum).

Removing the propagation of scattered Rayleigh waves between imaging points and receivers [accounted for by the Green's function V^G of equation (2)] can also be simplified. To this aim, we assume all scattering objects to be lumped at the receiver line and discard the integration over the transverse horizontal direction (the y-direction). After imaging, all objects directly below the line will be imaged at time $t = 0$, whereas objects close to the line (at distances not exceeding a wavelength) will be imaged at somewhat later times τ, given by

$$\tau = \frac{y}{|c_R|}, \tag{5}$$

where y is the lateral distance of the object from the receiver line. Since the operator given by equation (3) is not strictly correct for $y > 0$, these objects will not be imaged perfectly; however, for lateral distances not exceeding a wavelength, this will probably be a minor effect. After wavefield separation of the incident field, v_0, we obtain the scattered field v_1; the result is shown in Figure 4. This separation has been carried out separately for the different shots (after correcting for the propagation delay from the shot locations to the scattering region). The results for the different shots are very similar, which implies that the scattered field shown in Figure 4 is shot generated and not the result of ambient noise. The slopes visible in Figure 4 are associated with the Rayleigh-wave speed, giving us a good indication that we indeed extracted the scattered Rayleigh waves.

After imaging the scattered field by spatially deconvolving for the Green's function V^G and performing a temporal deconvolution for the total field v [see also equation (2)], we obtain the impedance function (Figure 5), displayed as a function of receiver coordinate and time. At about 53 m, we see the image of the root system of the bush at a traveltime of 8 ms, implying a horizontal distance of 2 m, which is consistent with the surface location of the bush. The width of the image is approximately 1–2 m. Since the Rayleigh-wave speed ($|c_R|$) is about 240 m/s and the dominant frequency of the Rayleigh waves is about 35 Hz, the dominant Rayleigh wavelength is approximately 7 m.

There also appears to be another image at a horizontal receiver distance of 35 m. From the image time, we conclude that the cross-line distance between the scattering object and the line is about 1.5 m. Since the object has no surface manifestation, we do not know what it is. The size seems to be 1–2 m along the receiver line. Most important, there appears to be no image of the buried drum. The data set that was recorded prior to burying the drum resulted in an image nearly identical to the one shown in Figure 5. From this experiment, we conclude that, in this case, we were able to image scattering objects down to sizes of 1–2 m that are at a maximum distance of 3 m from the receiver line. No objects were imaged at larger distances, and it seems likely that the near-receiver scattering process dominates all other near-surface scattering processes in this vertical-component data set.

INTERPRETATION OF THE CROSS-LINE HORIZONTAL-COMPONENT DATA

Because of the elliptic polarization of Rayleigh waves, cross-line horizontal-component geophones should be about as sensitive to cross-line scattered Rayleigh waves as the vertical-component geophones. At the same time, the cross-line component is less sensitive to in-line polarized waves, like the illuminating guided wave directly from the source (Blonk and Herman, 1996). The cross-line component is also less sensitive to in-line, or almost in-line, scattered Rayleigh waves originating from heterogeneities close to the line (like the bush at 53 m, in our case). Because of the reduced sensitivity of the cross-line horizontal component to the illuminating guided wave and the in-line scattered waves from heterogeneities very close to the line, one might expect that this cross-line component could be used to image objects at somewhat larger distances from the line. One of the cross-line horizontal shot records after the drum burial is shown in Figure 6. In principle, a similar processing sequence would be possible for the horizontal-component data as for the vertical component data. In our experiment, however, the horizontal-component data quality was considerably inferior to the vertical-component data, and

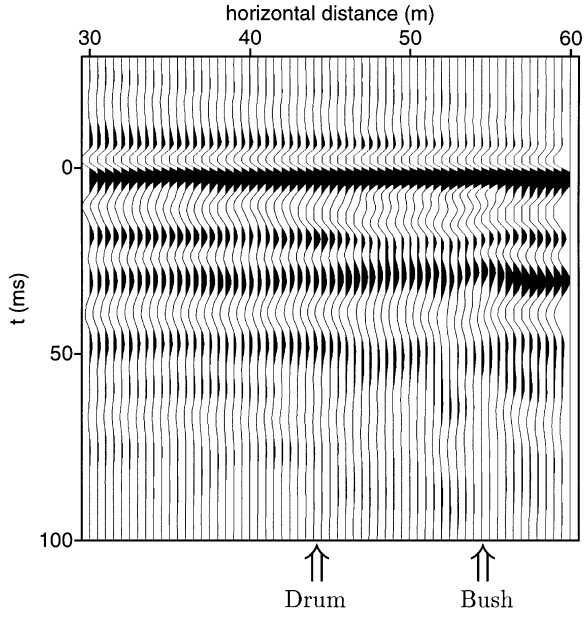

FIG. 3. The total wavefield, v, for the data set recorded after burying the drum. The effect of propagation of the guided wave from each shot to the region close to the receiver line has been removed by aligning the traces on their first-break times, after which the shots have been stacked.

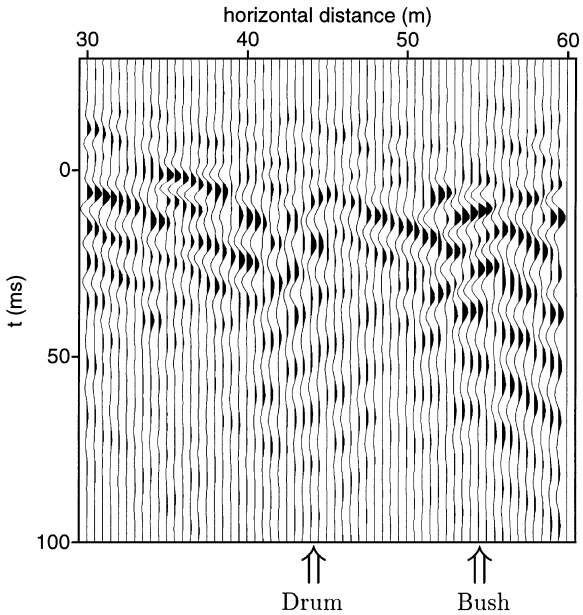

FIG. 4. The scattered field, v_1, obtained after wavefield separation of the incident field from the scattered field. The dominant Rayleigh-wave velocity appears to be $|c_R| = 240$ m/s (the traces are still aligned on the first-break picks).

good first-arrival picks could not be obtained. Therefore, the only processing carried out on the horizontal-component data was killing the bad traces, followed by bandpass filtering and f–x deconvolution to enhance spatial coherency and suppress noise. If three-component geophones had been used, we could have used the vertical-component picks; a similar data processing sequence might have been possible as for the vertical-component data.

The cross-line horizontal data shown in Figure 6 show evidence of a diffraction tail, originating from the bush at 53 m, and a faint hyperbola, centered at 44 m, with its apex arriving at about 120 ms (i.e., 40 ms after the first arrival). Using the Rayleigh-wave velocity of 240 m/s, this suggests a lateral distance of about 10 m. This hyperbola was also quite consistently visible on the other horizontal records. Unfortunately, we did not record the horizontal data before burying the drum, so no definite conclusions can be drawn whether this scattering hyperbola is because of the drum or another heterogeneity. Nevertheless, it appears one can see objects up to 10 m away and that the cross-line data are indeed more sensitive to cross-line scattered Rayleigh waves than the vertical-component data. In the cross-line data, the first arrival as well as the (almost) in-line scattered waves from the bush and the heterogeneity at 35 m are weaker.

CONCLUSIONS

We have discussed a method for imaging very shallow objects at a relatively small distance from the receivers. As an illuminating wave, the first arrival (guided) wave is used. This illuminating wave is converted into scattered Rayleigh waves at shallow heterogeneities. From the field experiment carried out at the Richmond Field Station, we found that we could use the vertical component data to image objects of size 1–2 m at a maximum distance of 3 m from the receiver line. Objects farther away could not be imaged because of the dominant presence of scattered waves from these nearby heterogeneites. This scattering possibly resulted from the presence of mud cracks. Even though the ground appeared well saturated, deep mud cracks were visible at the surface in some places, these being a result of the previous dry summer.

The cross-line horizontal data appear to be more sensitive to cross-line scattered Rayleigh waves and less sensitive to the illuminating guided wave and in-line scattered waves. This type of data could therefore enable one to maybe detect objects somewhat farther away, but the evidence is lacking to make

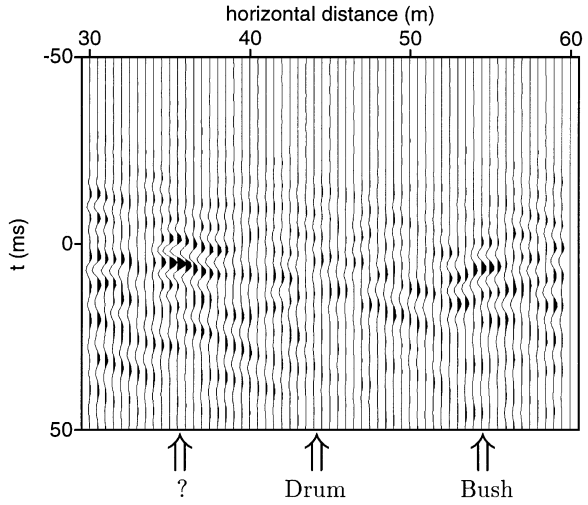

FIG. 5. After imaging the scattered field as a function of receiver coordinate and time t, we obtain the impedance function shown here. At about 53 m, we see the image of the root system of the bush at a traveltime of about 8 ms, implying a horizontal distance of about 2 m, which is consistent with the surface location of the bush. The width of the image is 1–2 m. There also appears to be another image at a horizontal receiver distance of about 35 m. From the image time, we conclude that the cross-line distance between the scattering object and the line is about 1.5 m. Since the object has no surface manifestation, we do not know what it is. The size seems to be 1–2 m along the receiver line. There appears to be no image of the buried drum from the vertical component of the data.

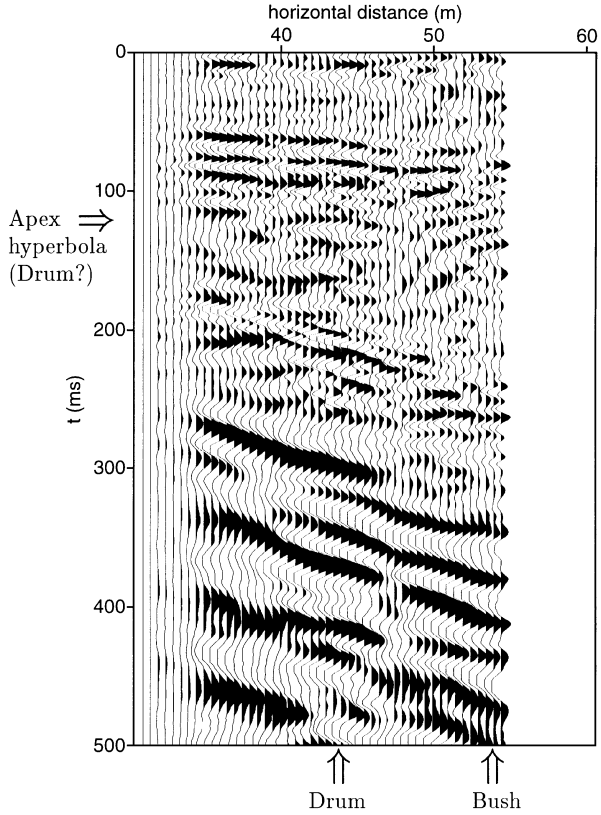

FIG. 6. A typical 48-channel recording of the cross-line horizontal component after the drum burial. Apart from a diffraction tail originating from the bush at 53 m, we see a faint hyperbola centered at 44 m, with its apex arriving at 120 ms—40 ms after the first arrival. Using a Rayleigh-wave velocity of 240 m/s, this suggests a lateral distance of about 10 m. This hyperbola was also quite consistently visible on the other horizontal records. It seems one can see objects up to a distance of 10 m, and that the cross-line data are more sensitive to cross-line scattered Rayleigh waves than the vertical component data. The first arrival occurs at about 80 ms, the airwave starts at about 180 ms, and the low-frequency ground roll (Rayleigh wave) starts at about 270 ms.

firm statements based on this experiment. It is, however, consistent with earlier findings (Blonk and Herman, 1996). The results might be improved by using three-component geophones and measuring the Green's function by a few separate short-offset experiments with a low-energy source. Other experiments showed that the Rayleigh wave could also be used as the illuminating field (Blonk et al., 1995) and that a dam could be imaged at a distance of 150 m, whereas for another data set, objects could be imaged at distances of more than 1 km. The possibility of detecting shallow objects is therefore very dependent upon the size of the object, their contrast, and the properties of the shallow subsurface. We consider this as a pilot study showing some of the potential of the imaging of shallow objects using scattered guided waves, and we intend to investigate both theoretical (modeling) and experimental aspects in more detail in the near future. At this pont, we cannot yet make a meaningful comparison between our seismic method and EM or ground-penetrating radar (GPR) methods, which are very popular for investigating the shallow subsurface. In any case, a significant difference is that the seismic method is sensitive to mechanical contrasts that might be relevant for geotechnical applications, whereas EM and GPR methods are sensitive to contrasts in electrical properties.

ACKNOWLEDGMENTS

This research was conducted while G. H. was a Phoebe Apperson Hearst visiting professor in the Dept. of Materials Science and Mineral Engineering with the financial support of the University of California at Berkeley and the Dutch Technology Foundation. This support is gratefully acknowledged. The Richmond Field data were obtained with the help of John Washbourne, Qicheng Dong, and Tao Zhen of the Engineering Geoscience Group at the Lawrence Berkeley National Laboratory. Their assistance was valuable in this "Dutch day in the field" with a lot of rain and mud. More details and action pictures can be found at http://bozo-1.lbl.gov/users/paul/RFS/Dutchday.html. The equipment used during the experiment was made available by Geometrics Inc. The seismic data were processed using software donated by Landmark Graphics Corp. as part of its strategic alliance with Univ. of California, Berkeley.

REFERENCES

Berkhout, A. J., 1985, Imaging of acoustic energy by wavefield extrapolation, 3rd ed.: Elsevier Science Publ. Co., Inc.

Blonk, B., and Herman, G. C., 1994, Inverse scattering of surface waves: A new look at surface consistency: Geophysics, **59**, 963–972.

——— 1996, Removal of scattered surface waves using multicomponent seismic data: Geophysics, **61**, 1483–1488.

Blonk, B., Herman, G. C., and Drijkoningen, G. G., 1995, An elastodynamic inverse scattering method for removing scattered surface waves from field data: Geophysics, **60**, 1897–1905.

Ernst, F. E., and Herman, G. C., 1998, Removal of guided waves from seismic data in laterally varying media: Wave Motion, **28**, 173–189.

Mars, J. I., and Rector, J. W., 1995, Constrained eigenvectors: A means to separate aliased arrivals: 65th Ann. Internat. Mtg., Soc. Expl. Geophys., Expanded Abstracts, 49–52.

Steeples, D. W., Green, A. G., McEvilly, T. V., Miller, R. D., Doll, W. E., and Rector, J. W., 1997, A workshop examination of shallow seismic reflection surveying: The Leading Edge, **16**, 1641–1647.